Various Architectures of Colloidal $Cu_3(MoO_4)_2(OH)_2$ and $Cu_3Mo_2O_9$; Thermal Stability, Photoluminescence and Magnetic Properties of $Cu_3(MoO_4)_2(OH)_2$ and $Cu_3Mo_2O_9$ Nanosheets

Azam Bayat [a,*], Ali Reza Mahjoub [a] , Mostafa M. Amini[b]

[a]Department of Chemistry, Tarbiat Modares University, Tehran 14155-4383, Iran

[b]Department of Chemistry, Shahid Beheshti University, G. C., Tehran 198396311, Iran

Corresponding author: Azam Bayat

E-mail address: azam.bayat @modares.ac.ir

[DOI: 10.22068/ijmse.3916]

Abstract

The lindgrenite compounds [$Cu_3(MoO_4)_2(OH)_2$] with various architectures and high crystallinity were prepared by a simple surfactant-assisted hydrothermal method. Then, the $Cu_3Mo_2O_9$ samples were prepared by calcination of the as-synthesized $Cu_3(MoO_4)_2(OH)_2$. The resulting samples exhibited high crystallinity, colloidal properties, a high yield, and a large-scale production capability, all achieved using nontoxic and inexpensive reagents, as well as water, which serves as an environmentally friendly solvent. The scanning electron microscope studies showed that the as-prepared Lindgrenite nanostructures were well crystallized with rod, sheet and hollow sphere morphologies. These products were content of the $Cu_3(MoO_4)_2(OH)_2$ rods with diameters of about 100 nm, the $Cu_3(MoO_4)_2(OH)_2$ nanosheets with thickness of 30–100 nm and the $Cu_3(MoO_4)_2(OH)_2$ hallow spheres, consisting of a large number of nanosheets with thickness of about 40-70 nm. The $Cu_3Mo_2O_9$ samples obtained by thermal treatment of Lindgrenite retained the original morphologies. Meanwhile, the photoluminescence and magnetic properties of the nanosheet samples exhibited superparamagnetic behaviour at room temperature. In comparison with previous works, the Cu3(MoO4)2(OH)2 and Cu3Mo2O9 samples synthesized by the surfactant-assisted hydrothermal method exhibited a pronounced red-shifted PL emission and high intensity.

Keywords: $Cu_3(MoO_4)_2(OH)_2$; $Cu_3Mo_2O_9$; colloidal; super paramagnetic; red emission

1. INTRODUCTION

Molybdenum oxide-based materials, especially binary ones, have received considerable attention due to their applications in catalysts, display devices, photochromism, sensors, batteries, absorption, electrical conductivity, magnetism, photochemistry and smart windows [1-2].

Lindgrenite is a rare mineral initially discovered in Chile, resulting from the oxidation of primary molybdenite [3]. The preparation of natural minerals is useful for verifying the quality of minerals and determining the geological origin of mineral formation. The structural and compositional determination of synthetic mineral crystals may establish standards for evaluating the quality of natural minerals. Furthermore, the synthetic approach may facilitate the large-scale production of low-cost, high-quality natural minerals, particularly those with technological and economic interest but are rare or impure in nature. The study of conditions for mineral formation helps mineralogists explore minerals in specific zones where geological reactions once occurred under similar circumstances mentioned above [4]. Lindgrenite is an effective fire retardant and smoke suppressor when combined with $CuSnO_3$ in polyvinyl chloride plastic (PVC). For this purpose, it appears that needle-like and sheet-like structure materials are suitable candidates for functional polymeric composites and fibre hybrid materials [5-6].

On the other hand, the properties of $Cu_3Mo_2O_9$ have attracted extensive interest in various research fields [1]. Molybdenum trioxide nanostructures can be used as catalysts. For instance, $Cu_3Mo_2O_9$ is employed in the deep oxidation of diesel exhaust with high activity, but reports on $Cu_3Mo_2O_9$ morphologies are very few [2, 7].

Shores et al. have reported the synthesis of Lindgrenite elegantly modified by bipyridine and piperazine. The two ditopic ligands, interestingly, break the inorganic 3D network into layers, consequently transforming the ferromagnetic Lindgrenite into antiferromagnets. Vilminot et al. presented the hydrothermal synthesis of the hydrogenated and deuterated analogues of lindgrenite [8]. Bao et al. synthesized Cu3(MoO4)2(OH)2, which can be transformed into the metastable phase Cu3Mo2O9 through thermal decomposition. Xu et al. prepared $Cu_3Mo_2O_9$ with hollow and prickly sphere-like architecture by a simple thermal treatment of Lindgrenite. Also, Jiang et al.

synthesized Lindgrenite nanocrystals by simple aqueous precipitation, which could be decomposed to $Cu_3Mo_2O_9$. Hasan et al. synthesized $Cu_3Mo_2O_9$ for catalytic oxidation of the harmful gases, and Zhang et al. prepared $Cu_3Mo_2O_9$ nanosheets by a hydrothermal method and investigated the direct electrochemistry of hemoglobin (Hb). Finally, Xia et al. constructed $Cu_3Mo_2O_9$ nanoplates with excellent lithium storage properties based on a pH-dependent dimensional change [1, 9].

In this work, by a hydrothermal surfactant-assisted method, the colloidal $Cu_3(MoO_4)_2(OH)_2$ and $Cu_3Mo_2O_9$ nanorods, nanosheets and self-assembled hollow spheres with high crystallinity were synthesized. A significant feature of this synthetic approach is that the resulting samples have high crystallinity, a hydrophilic surface, a high yield, and a large-scale production capability using nontoxic and inexpensive reagents, as well as water, which serves as an environmentally benign reaction solvent. For the use of these nanostructures in applied sciences, it is necessary for them to be dispersible or soluble in water, and the solubility and dispersibility of the samples play a key role in their applications. The size and shape of the as-synthesized samples can be readily controlled by adjusting the reaction parameters, which significantly influence the morphologies of the final samples. Meanwhile, possible growth mechanisms for the formation of single-crystalline $Cu_3(MoO_4)_2(OH)_2$ products were proposed. Moreover, the photoluminescence and magnetic properties of the as-synthesized $Cu_3(MoO_4)_2(OH)_2$ and $Cu_3Mo_2O_9$ nanosheets were determined in which a red emission was observed at 706 nm by excitation at 237 nm in their photoluminescence spectra of the $Cu_3(MoO_4)_2(OH)_2$ and $Cu_3Mo_2O_9$ at room temperature. Additionally, the results of the magnetic properties investigation of the Cu3(MoO4)2(OH)2 and Cu3Mo2O9 nanosheet samples revealed that these nanosheet samples exhibit superparamagnetic behavior at room temperature. Nanosheet morphology exhibits a unique feature of two-dimensional anisotropy,

[DOI: 10.22068/ijmse.3916]

which triggers quantum confinement effects, thereby gaining new physicochemical properties. This morphology has important applications in the field of energy conversion, storage devices, biological sensors, electronics, ferromagnetic, magneto-optical, electrochemical, photo-responsive, flexible electrochromic devices, biotechnology, water splitting, catalysis, gas sensing, and energy storage due to their unique electric properties and high packing densities [10-14].

2. EXPERIMENTAL PROCEDURES

2.1. Materials and Apparatus

All of the raw materials used in this research, except $Cu(NO_3)_2.3H_2O$ (Panreac), were purchased from Merck. The structure and phase purity of as-synthesized samples were characterized by X-ray diffraction (XRD) on a Philips X'pert X-ray diffractometer using Cu Kα radiation (wavelength, $\lambda = 1.5418$ Å). Fourier transform infrared (FT-IR) spectra of samples were recorded on a Shimadzu-8400S spectrometer in the range of 400–4000 cm^{-1} using KBr pellets. The scanning electron microscopy (SEM) analysis of Lindgrenite ($Cu_3(MoO_4)_2(OH)_2$) and $Cu_3Mo_2O_9$ was performed using a TESCAN (VEGA3) instrument. Thermogravimetric analysis (TGA) and differential thermal analysis (DTA) were performed on a STA 504; the atmosphere was air. Photoluminescence (PL) spectra of the nanosheet samples were recorded on a JASCO FP-6500 spectrofluorometer at room temperature. Finally, the magnetic properties of the nanosheet samples were measured at room temperature using a vibrating sample magnetometer (VSM; Meghnatis Kavir Kashan Co., Kashan, Iran) in a maximum applied field of 15 kOe.

2.2 Synthesis of $Cu_3(MoO_4)_2(OH)_2$ Nanorods

For the synthesis of Lindgrenite nanorods, $Cu(NO_3)_2.3H_2O$ (0.42 g, 1.74 mmol), $Na_2MoO_4.2H_2O$ (0.28 g, 1.16 mmol) and 6-aminohexanoic acid (0.46 g, 3.51 mmol) were dissolved in 140 mL

[DOI: 10.22068/ijmse.3916]

distilled water. The mixture was stirred for 10 min at room temperature. Precipitates were produced immediately from the combination of the metal cation (Cu^{2+}) and molybdate anion (MoO_4^{2-}) at a pH of 5, the initial pH of the solution. The resulting reaction mixture (140 mL) was transferred to a 200 mL Teflon-lined stainless steel autoclave and heated to 180°C for 20 hours. The obtained samples were filtered, washed with distilled water, and dried at 60 °C for 2 h or more.

2.3 Synthesis of $Cu_3(MoO_4)_2(OH)_2$ Nanosheets

Moreover, for the synthesis of lindgrenite nanosheets, $Cu(NO_3)_2.3H_2O$ (0.23 g, 0.96 mmol) and 6-aminohexanoic acid (0.50 g, 3.84 mmol) were dissolved in 63 mL distilled water. A 0.03 M aqueous solution of sodium molybdate (63 mL) was added to the above solution at room temperature, stirring for 10 minutes. The resulting reaction mixture (126 mL) was transferred to a 220 mL Teflon-lined stainless steel autoclave and treated to 180 ºC for 20 h. The obtained samples were filtered, washed with distilled water, and dried at 60 °C for 2 h or more.

2.4 Synthesis of $Cu_3(MoO_4)_2(OH)_2$ Hollow Spheres

Finally, for the synthesis of Lindgrenite hollow spheres, Cu(NO3) 2 · 3H2O (0.42 g, 1.74 mmol) and 6-aminohexanoic acid (0.46 g, 3.51 mmol) were dissolved in 57 mL of distilled water. A 0.015 M aqueous solution of sodium molybdate (57 mL) was added to the above solution at room temperature, stirring for 10 min. The resulting reaction mixture (114 mL) was transferred to a 200 mL Teflon-lined stainless steel autoclave and treated to 60 ºC for 20 h. The obtained samples were filtered, washed with distilled water, and dried at 60 °C for 2 h or more.

2.5 Synthesis of $Cu_3Mo_2O_9$ with Various Architectures

For the synthesis of $Cu_3Mo_2O_9$ with various architectures, the as-synthesized $Cu_3(MoO_4)_2(OH)_2$ samples directly calcined in a furnace at calcination temperature of 500 °C, in air for 4 h with a heating rate of 10 °C min^{-1}.

3. RESULTS AND DISCUSSION

3.1 Structure and Morphology of $Cu_3(MoO_4)_2(OH)_2$

The structure of Lindgrenite is composed of $Cu_3(OH)_2$ ribbons of the brucite structure, consisting of edge-sharing copper octahedra with two kinds of copper atoms, Cu(1) and Cu(2), both having distorted octahedral coordination of oxygen atoms, running parallel to the *c-axis*. MoO_4 connects three ribbons together via its oxygen atoms: O(1) and O(3) are bonded to single Cu atoms, while O(2) and O(4) bridge two copper atoms each on two adjacent chains [15]. Fig. 1 shows the XRD patterns of lindgrenite samples prepared by hydrothermal surfactant-assisted synthesis. Lindgrenite ($Cu_3(MoO_4)_2(OH)_2$) crystallizes in a monoclinic system with the space group of $P2_1/n$ (No. 14) [15]. Diffraction patterns of all $Cu_3(MoO_4)_2(OH)_2$ samples are well-indexed to the monoclinic phase structure, and they are in accordance with the JCPDS card no. 75-1438 (Fig. 1). The intense diffractions in patterns without any other peaks indicate the high purity and well-crystallinity of the samples. The eight primary reflections; 12.62°, 20.42°,21.34°, 24.85°, 25.34°, 25.42°, 25.62° and 33.43° are indexed as (020), (021), (101), (121), (130), (040), (111) and (141) of $Cu_3(MoO_4)_2(OH)_2$, respectively, and they are in agreement with the data reported in literature [16].

[DOI: 10.22068/ijmse.3916]

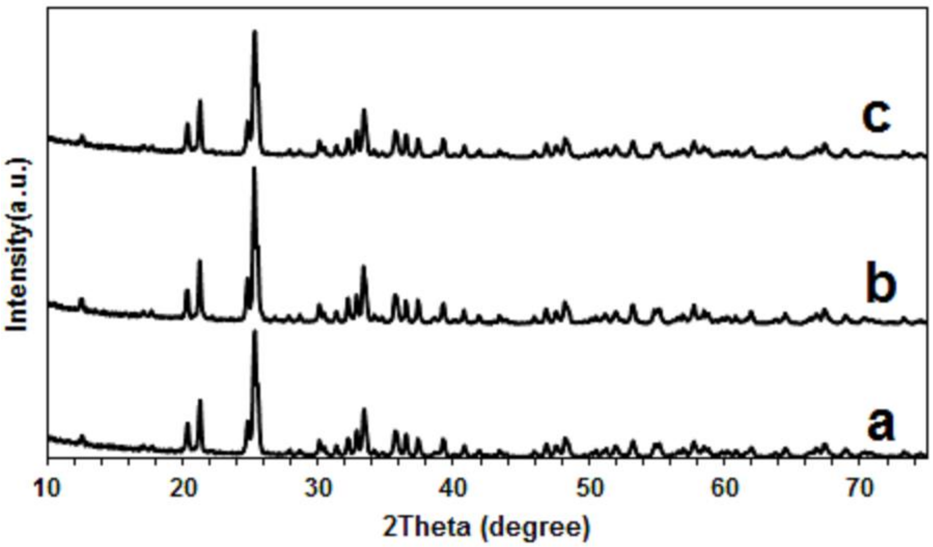

Fig. 1. XRD patterns for the $Cu_3(MoO_4)_2(OH)_2$ samples with (a) rod, (b) sheet and (c) hollow spherical shapes.

The FTIR spectra of the colloidal $Cu_3(MoO_4)_2(OH)_2$ samples are shown in Fig. 2a-c. The bands at approximately 800-1000 cm−1 are attributed to the MoO42− stretching vibration, which is consistent with the reported values [8]. The band at about 450 cm^{-1} is assigned to the bending vibration of Cu-O. Additionally, the weak absorptions at approximately 1600 cm−1 and the bands at 3000–3600 cm−1 indicate the bending and stretching vibrations of H_2O, respectively, as well as the O-H bond [17-18]. Bands at about 2800-2900 cm^{-1} are attributed to the C-H stretching vibrations of methylene groups of the AHA molecules, which have been overlapped with the stretching vibration of H_2O bands, and bands at about 1400 cm^{-1} correspond to C-N bending modes of AHA molecules. Meanwhile, Bands at about 3400 cm^{-1} correspond to the $-NH_2$ stretching mode of AHA molecules [19-22]. These results demonstrate that the carboxylic (-COOH) terminus is free and thus, approves hydrophilicity of the three samples.

[DOI: 10.22068/ijmse.3916]

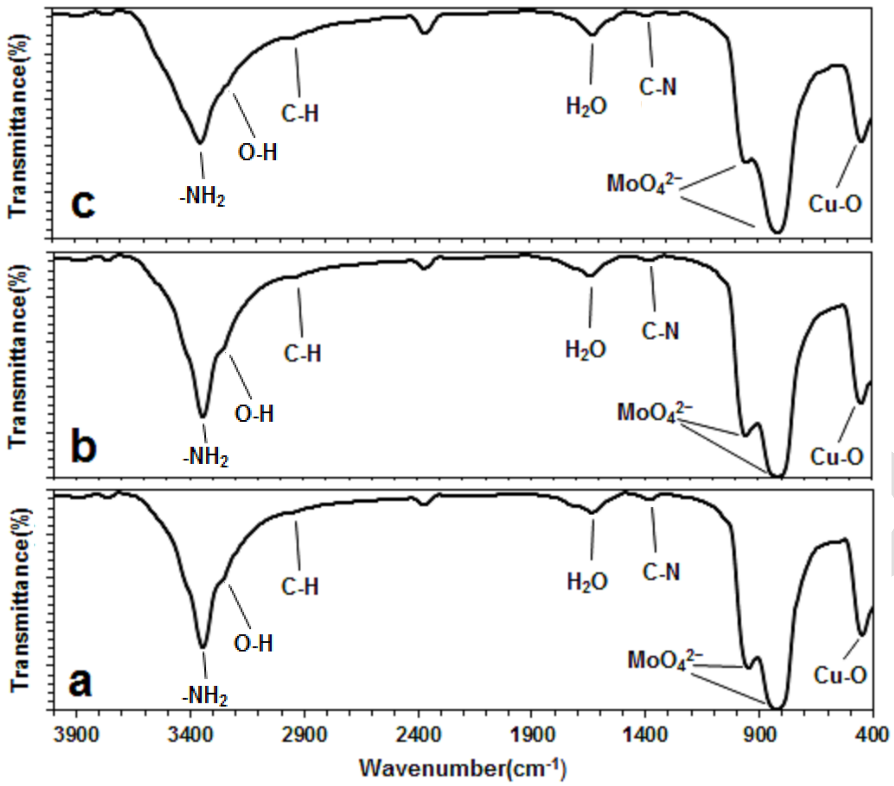

Fig. 2. Infrared spectra of the as-prepared colloidal $Cu_3(MoO_4)_2(OH)_2$ with various architectures: (a) rod, (b) sheet and (c) hollow sphere morphology.

The morphologies of the as-prepared products were also examined by SEM (Fig. 3). Fig. 3a-b show SEM images of the prepared Cu3(MoO4)2(OH), which has a rod morphology with diameters of approximately 100 nm. Fig. 3c-e shows the SEM image of Cu3(MoO4)2(OH)2 prepared from a 0.03 M aqueous solution of sodium molybdate at 180 °C. As the Figures show, the as-synthesized sample has sheet forms with sizes ranging from 30 to 100 nm in width. The SEM observation also indicates that almost 100% of the obtained $Cu_3(MoO_4)_2(OH)_2$ sample is a super-thin sheet, and no other type of particle is visible. Fig. 3f shows an SEM image of the $Cu_3(MoO_4)_2(OH)_2$ prepared with a 0.015 M aqueous solution of sodium molybdate at 60°C, in which the as-synthesized sample has a hollow sphere architecture. The mean diameter of these hallow spheres were about 25 μm as

[DOI: 10.22068/ijmse.3916]

shown in Fig. 3g. Moreover, SEM image of the $Cu_3(MoO_4)_2(OH)_2$ hallow spheres demonstrate which an individual hallow sphere is composed of a large number of nanosheets with a thickness of about 40-70 nm (Fig. 3h). Also, the SEM observation shows that the spheres have hollow structures (Fig. 3i).

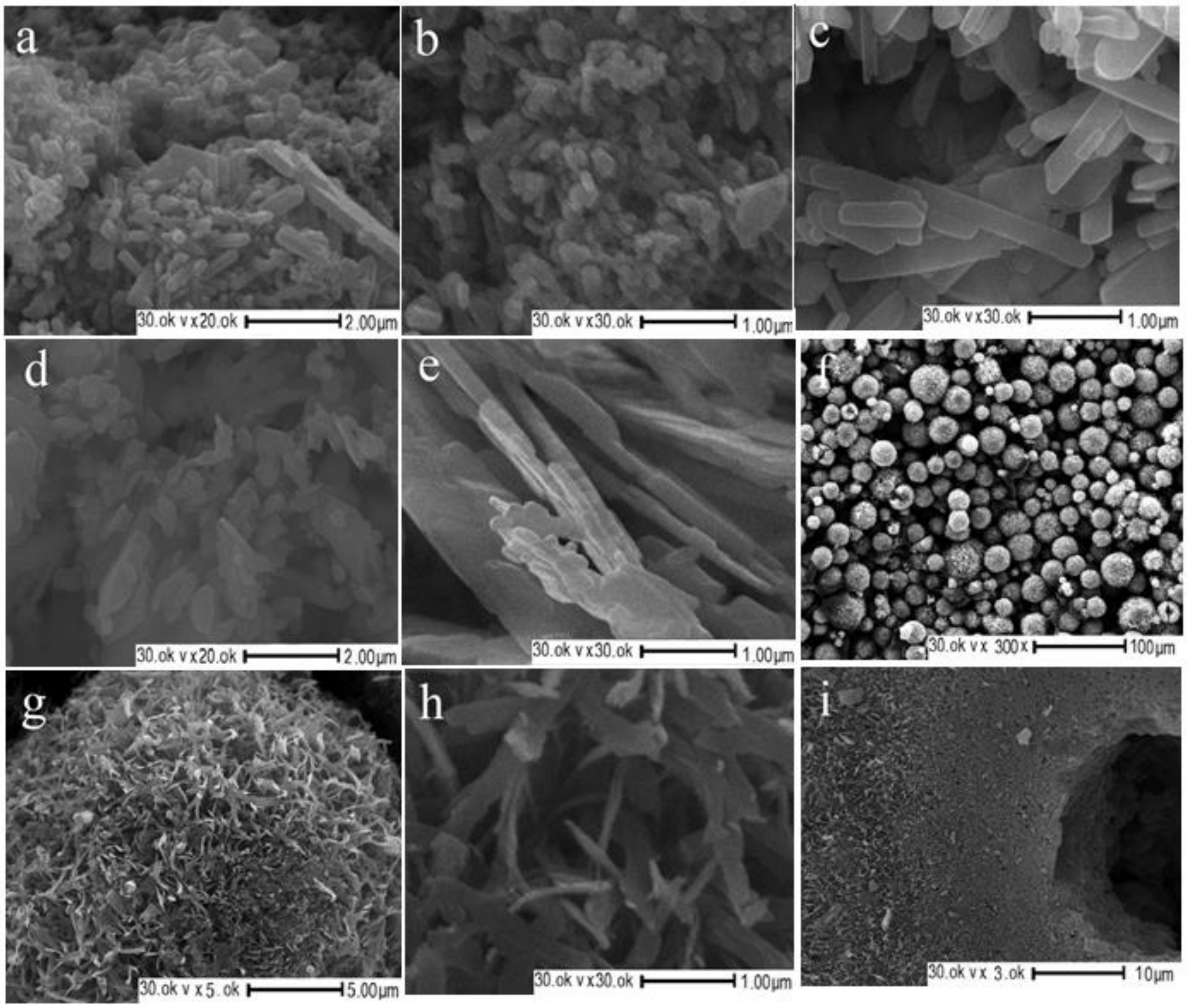

Fig. 3. SEM images of (a-b) $Cu_3(MoO_4)_2(OH)_2$ rod-shaped structure, (c-e) $Cu_3(MoO_4)_2(OH)_2$ sheet form structure, (f-i) $Cu_3(MoO_4)_2(OH)_2$ hollow spherical shape.

[DOI: 10.22068/ijmse.3916]

[DOI: 10.22068/ijmse.3916]

3.2 Possible Growth Mechanism of $Cu_3(MoO_4)_2(OH)_2$ with Various Architectures

For $Cu_3(MoO_4)_2(OH)_2$ nanorods, the proposed mechanism, based on literature reports, involves two well-known mechanisms: Ostwald ripening and oriented attachment [23-24]. When $Cu(NO_3)_2.3H_2O$ solution was added to the MoO_4^{2-} solution in the presence of 6-aminohexanoic acid, $Cu(OH)_2$ formed first. Then $Cu(OH)_2$ combined with copper ions and MoO_4^{2-} and a high supersaturation degree will be reached, and amorphous $Cu_3(MoO_4)_2(OH)_2$ particles will form immediately. This process is described in Equations (1) and (2) [25].

$Cu^{2+} + 2OH^{-} \rightarrow Cu(OH)_2$ (1)

$Cu(OH)_2 + 2Cu^{2+} + 2MoO_4^{2-} \rightarrow Cu_3(MoO_4)_2(OH)_2$ (2)

When the synthesis temperature was increased, monodisperse spherical nanoparticles were obtained. At a longer reaction time, the equilibrium of growth kinetics was observed and at higher reaction temperatures, according to the well-known Ostwald ripening process, a mixture of spherical particles and primary rod-like particles was observed and finally, with the temperature increasing of the reaction, no nanoparticles were observed. At elevated temperature, the nanorods involved thicker and longer colloidal nanorods. At this stage, the oriented attachment is the dominant mechanism [23].

On the other hand, for $Cu_3(MoO_4)_2(OH)_2$ nanosheets, based on literature reports [26-27], was considered that the molybdate nanosheets formation can be the effect of among Ostwald ripening [28], lateral-aggregation [23], and dissolution/recrystallization [26] processes. This is probably due to the presence of 6-aminohexanoic acid molecules in the water medium. Similar to rod morphology, when $Cu(NO_3)_2.3H_2O$ solution was added to the MoO_4^{2-} solution in the presence of 6-aminohexanoic acid, $Cu(OH)_2$ formed first. Then $Cu(OH)_2$ combined with copper ions and

MoO_4^{2-} and a high supersaturation degree will be reached, and amorphous $Cu_3(MoO_4)_2(OH)_2$ particles will form immediately. The interesting transformation of a small crystalline nucleus into Lindgrenite nanoparticles in a supersaturated solution at elevated temperature proceeds through the process known as Ostwald ripening. Subsequently, the primary nanoparticles quickly transform into Lindgrenite nanosheets through the lateral aggregation mechanism. At the end of the synthetic process, the shape transformation of the crystallized nanosheets often operates through a standard dissolution-recrystallization mechanism. Thus, the possible growth mechanism of the $Cu_3(MoO_4)_2(OH)_2$ nanosheets was dominated by a crystallization-dissolution-recrystallization mechanism.

For the self-assembled $Cu_3(MoO_4)_2(OH)_2$ hollow sphere sample, after formation of the subunit nanosheets *via* the proposed mechanism for Lindgrenite nanosheets, the assembly mechanism of sphere-like architecture operates. Therefore, the possible growth mechanism of the $Cu_3(MoO_4)_2(OH)_2$ hollow sphere morphology was dominated by a crystallization-dissolution-recrystallization- self-assembly growth mechanism.

3.3 Structure and Morphology of $Cu_3Mo_2O_9$

Tertiary copper molybdate, $Cu_3Mo_2O_9$, has an orthorhombic structure with space group *Pnma*. In the unit cell of this material, two types of Mo–4O tetrahedra, one compressed Cu-6O octahedral, and two types of Cu-5O polyhedral exist. The catalytic properties of this metal oxide are closely related to metal-oxygen bonds [2].

XRD patterns of the obtained $Cu_3Mo_2O_9$ with various architectures at a calcination temperature of 500 °C are shown in Fig. 4a-c. The diffraction patterns of the three Cu3Mo2O9 samples are well-

[DOI: 10.22068/ijmse.3916]

indexed to the orthorhombic structure and are in accordance with the standard diffraction patterns of Cu3Mo2O9, as listed in the JCPDS card number. 70-2493.

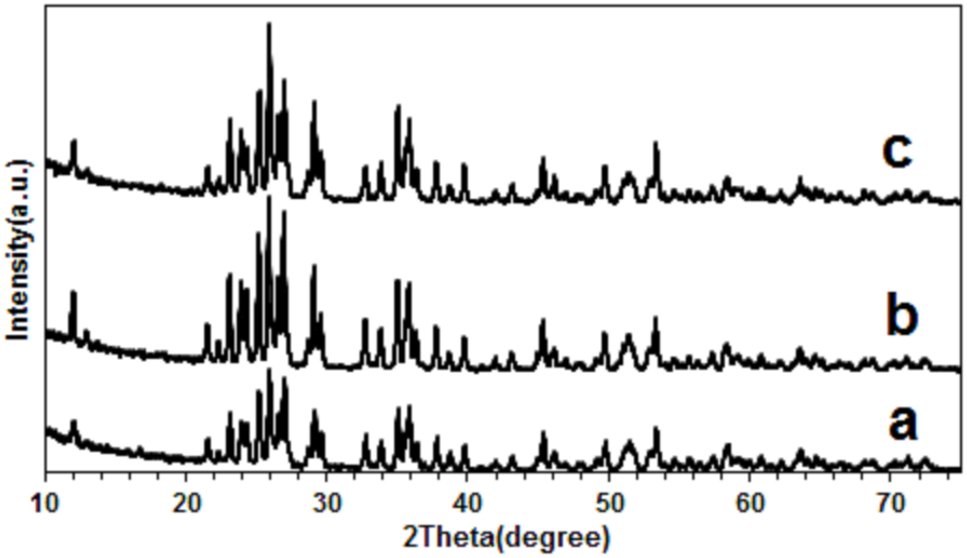

Fig. 4. XRD patterns of the $Cu_3Mo_2O_9$ samples calcined at 500 °C with (a) rod, (b) sheet and (c) hollow sphere morphologies.

The FTIR spectra of the colloidal $Cu_3Mo_2O_9$ samples are shown in Fig. 5a-c. Due to the difference of Cu–O and Mo–O bands in the crystal structures of $Cu_3(MoO_4)_2(OH)_2$ and $Cu_3Mo_2O_9$, in the spectra of $Cu_3Mo_2O_9$ samples, the excess bands appeared in the range of 400–1300 cm^{-1} [29-31]. The bands at 530 cm^{-1} are assigned to the bending vibration of the Cu−O bond. Additionally, the absorptions at 1600 cm−1 and the bands at 3000–3700 cm−1 indicate the bending and stretching vibrations of H_2O and O-H, respectively [16-18]. Bands at about 2800-2900 cm^{-1} are attributed to the C-H stretching vibrations of methylene groups of the AHA molecules, and bands at about 1400 cm^{-1} correspond to C-N bending modes of AHA molecules, respectively. Bands at about 3400 cm^{-1} correspond to $-NH_2$ stretching mode of AHA molecules, which have been overlapped with the stretching vibration of O-H bands [19-22]. These results support the hydrophilicity of the three

[DOI: 10.22068/ijmse.3916]

samples. As seen in Fig. 2, comparing with the bands of O-H stretching modes in $Cu_3Mo_2O_9$ samples, due to the existence of hydrogen bond in the Lindgrenite crystal lattice, the bands of O-H stretching modes in $Cu_3(MoO_4)_2(OH)_2$ samples have shifted to the lower wavenumbers and split into two bands.

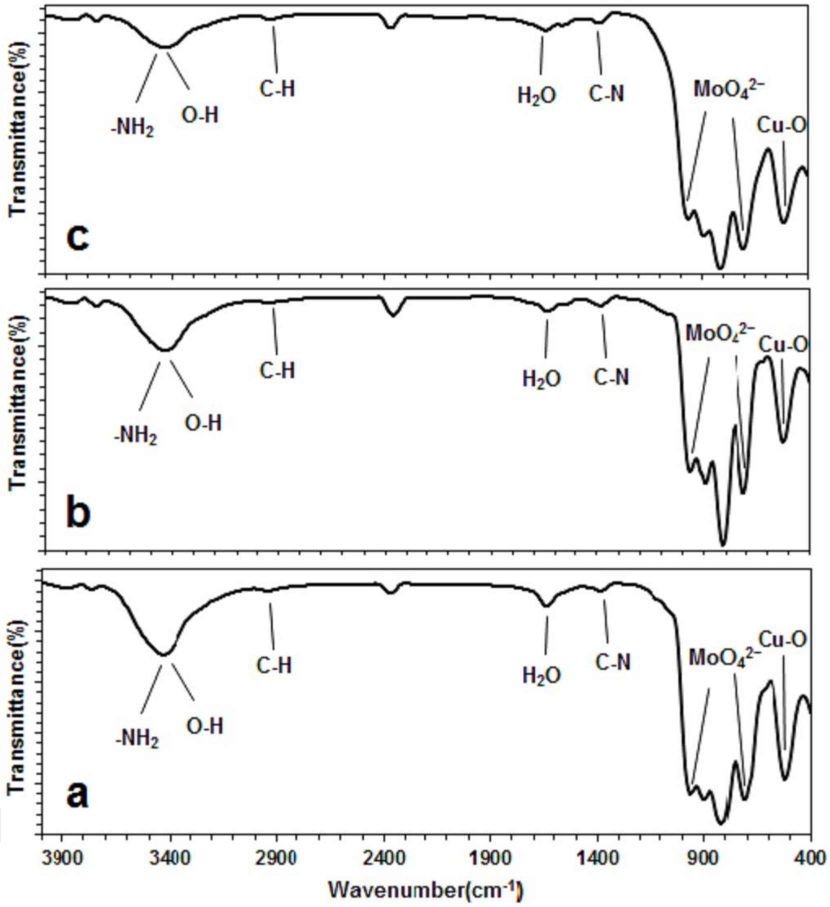

Fig. 5. Infrared spectra of the colloidal $Cu_3Mo_2O_9$ nanostructures: (a) rod, (b) sheet and (c) hollow sphere morphology.

SEM images of the $Cu_3Mo_2O_9$ samples obtained at calcination temperature of 500 °C, are shown in Fig. 6. SEM image of the $Cu_3Mo_2O_9$ obtained from calcined $Cu_3(MoO_4)_2(OH)_2$ nanorod sample is shown in Fig. 6a. As Figure shows the as-synthesized sample have rod forms with diameters of about 100 nm. Additionally, the SEM image of the Cu3Mo2O9 obtained from the calcined Cu3(MoO4)2(OH)2 nanosheet sample is shown in Fig. 6b and c. This sample retains the morphology of the Lindgrenite nanosheet sample, with a thickness of 20−100 nm. Finally, for the $Cu_3Mo_2O_9$ hollow sphere sample, calcined at 500 °C, the morphology of the Lindgrenite hollow sphere sample has been retained, with the same diameter of the hollow sphere and nanosheet thickness, which contributes to the hollow sphere structure, as shown in Fig. 6d-e.

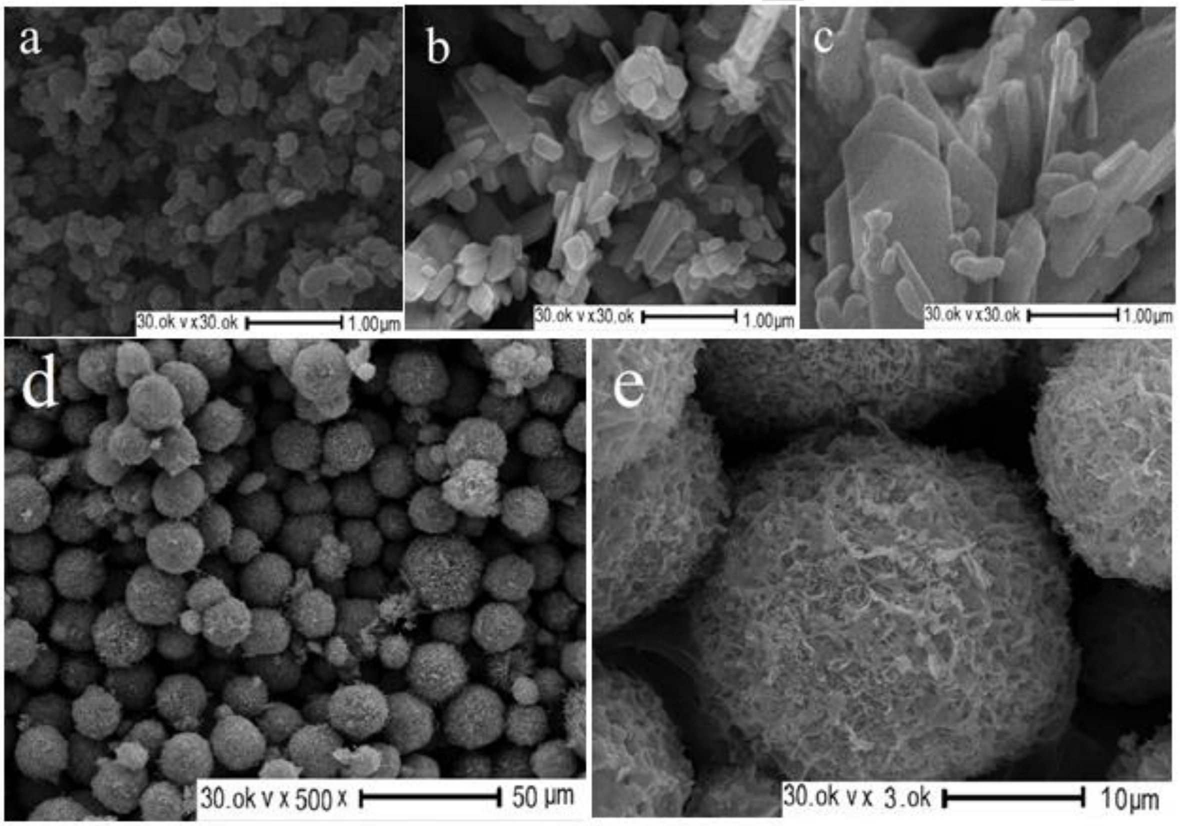

Fig. 6. SEM images of the colloidal $Cu_3Mo_2O_9$ (a) nanorods, (b-c) nanosheets and (d-e) hollow spheres.

3.4 Thermal Stability of $Cu_3(MoO_4)_2(OH)_2$ and $Cu_3Mo_2O_9$ Nanosheets

[DOI: 10.22068/ijmse.3916]

To investigate the thermal stability of Cu3(MoO4)2(OH)2 and Cu3Mo2O9, TG-DTA curves were obtained under a flow of air, as shown in Fig. 7. According to thermogravimetry (TG) analysis, the weight loss consists of two distinct steps. In the first stage, the TG curve indicated a weight loss (about 3.41 Wt%) between 50 °C and 450 °C, corresponding to the loss of adsorbed water and coordinated water [32] and elimination of OH groups as H_2O, resulting in the formation of $Cu_3Mo_2O_9$. Meanwhile, weight-loss steps in the range of 135 to 450 °C, corresponding to the combustion of 6-aminohexanoic acid of $Cu_3(MoO_4)_2(OH)_2$ surface [33]. A second weight loss was observed between 700 °C and 800 °C, corresponding to the decomposition of $Cu_3Mo_2O_9$. The three endothermic peaks in the DTA curve, at 171 °C, 384 °C, and 387 °C, are assigned to the loss of adsorbed water, coordinated water, and 6-aminohexanoic acid of $Cu_3(MoO_4)_2(OH)_2$, respectively. Finally, a significant endothermic peak at 780 °C resulted from the decomposition of $Cu_3Mo_2O_9$.

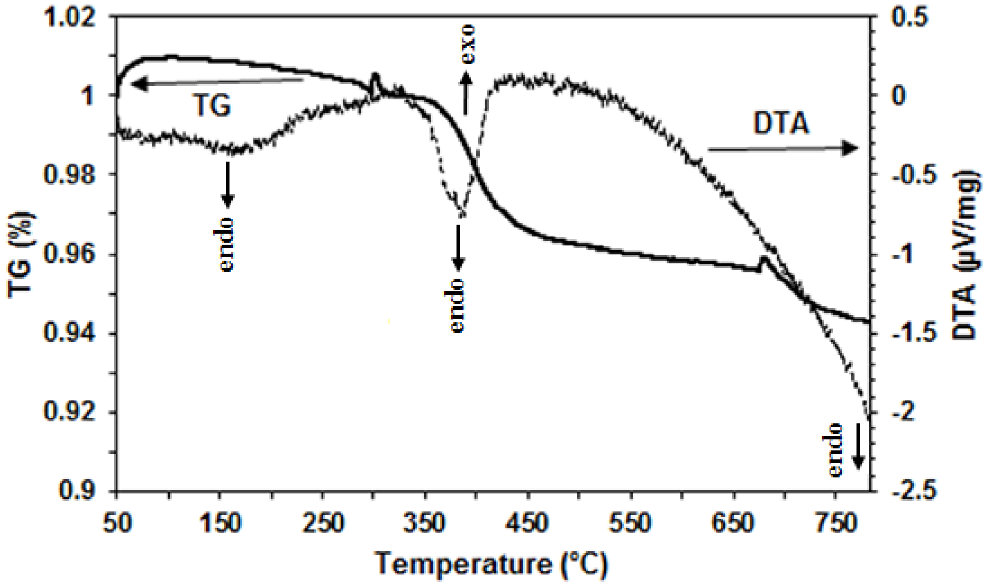

Fig. 7. TAG and DTA analysis of the prepared $Cu_3(MoO_4)_2(OH)_2$ and $Cu_3Mo_2O_9$ nanosheets.

3.5 Photoluminescence Properties of $Cu_3(MoO_4)_2(OH)_2$ Nanosheets

According to the earlier reports, $Cu_3(MoO_4)_2(OH)_2$ has the monoclinic structure with space group P$2_1/n$, and its crystal structure consists of strips of edge-sharing CuO6 octahedra that MoO42 cross-links$^-$ tetrahedral [3]. The MoO_4^{2-} tetrahedral is represented as $\Gamma_{Td} = A_1(v_1) + E(v_2) + F_2(v_3) + F_2(v_4)$ in which $A_1(v_1)$ and $E(v_2)$ are Raman active, but $F_2(v_3)$ and $F_2(v_4)$ are infrared active. Since the $F_2(v_3)$ vibrations are antisymmetric stretches, the bands at about 800 cm^{-1} are assigned to $F_2(v_3)$ antisymmetric stretching vibrations of $Cu_3(MoO_4)_2(OH)_2$. In this study, all samples exhibit the same bands at about 813 cm^{-1}. This band could originate from the Mo-O stretching vibration of the MoO_4 group [34].

Fig. 8 shows the room-temperature photoluminescence spectrum of the as-prepared $Cu_3(MoO_4)_2(OH)_2$ nanosheets using the excitation wavelength of 237 nm. The spectrum indicates that Lindgrenite nanosheets exhibit emission peaks at 705 nm, which may be attributed to charge-transfer transitions within the MoO_4^{2-} complex [35-39]. Compared with earlier results, the $Cu_3(MoO_4)_2(OH)_2$ sample synthesised in this work using the surfactant-assisted hydrothermal method exhibits a pronounced red-shifted PL emission. It is well known that the differences in maximum emission wavelengths can be attributed to the structural organisation levels, preparation methods, treatment conditions, and different excitation wavelengths, as well as the relative intensity of the emission peaks, which is closely related to morphology, size, surface defect states, and other factors [40-41]. Generally, these results indicate that the high-crystalline, hydrophilic-surfaced $Cu_3(MoO_4)_2(OH)_2$ nanosheets prepared in this work have potential as a photoluminescent material.

[DOI: 10.22068/ijmse.3916]

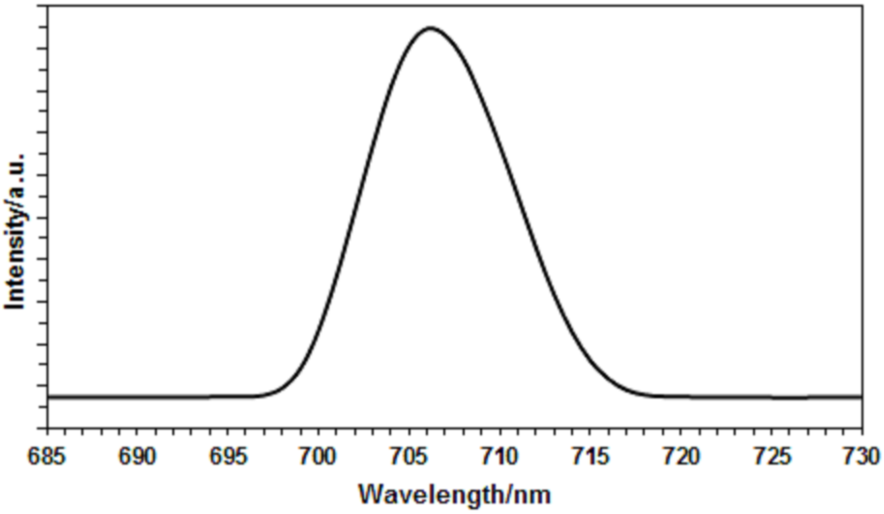

Fig. 8. Room-temperature photoluminescence spectrum of the prepared $Cu_3(MoO_4)_2(OH)_2$ nanosheet sample.

3.6 Magnetic Properties of $Cu_3(MoO_4)_2(OH)_2$ Nanosheets

The magnetization of our $Cu_3(MoO_4)_2(OH)_2$ nanosheets sample obtained by surfactant-assisted hydrothermal method as a function of magnetic field at the maximum field of 10 kOe is shown in Fig. 9. The magnetization of this sample is not completely saturated yet at the maximum field of the measurements (10 kOe). Hysteresis loops at room temperature are much thinner and reveal that the as-synthesized Cu3(MoO4)2(OH)2 nanosheets exhibit zero coercivity and, thus, are superparamagnetic at room temperature.

[DOI: 10.22068/ijmse.3916]

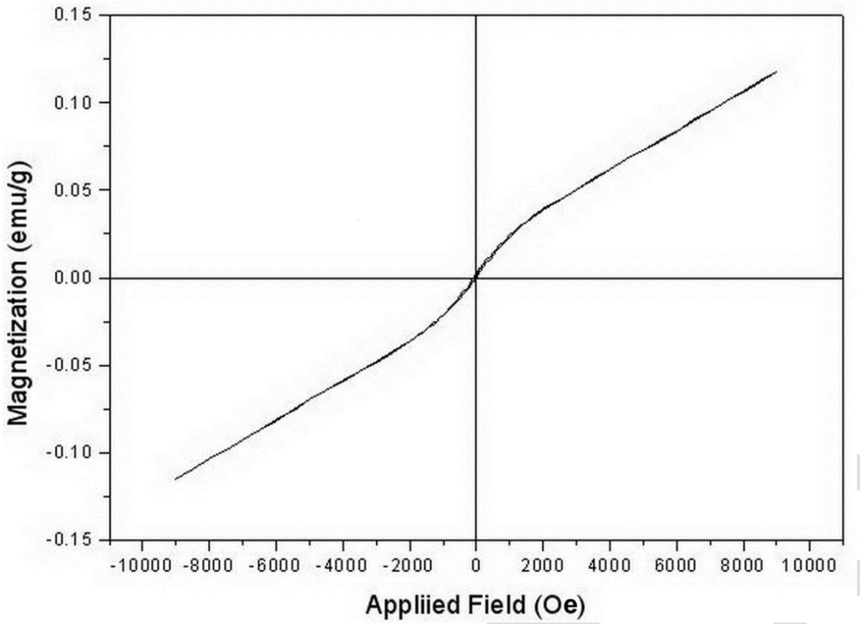

Fig. 9. Magnetic properties of the Lindgrenite nanosheets: magnetization vs. field and hysteresis loops of the sample at room temperature.

3.7 Photoluminescence Properties of $Cu_3Mo_2O_9$ Nanosheets

According to earlier reports, Cu3Mo2O9 has an orthorhombic structure with the space group Pnma. Within the unit cell of this material, two types of Mo-4O tetrahedra exist [2]. Fig. 10 shows the room-temperature photoluminescence spectrum of the as-prepared $Cu_3Mo_2O_9$ nanosheets using the excitation wavelength of 237 nm. The spectrum shows that the nanosheets exhibit emission peaks at 706 nm, which could be attributed to charge-transfer transitions within the MoO_4^{2-} complex [35-39]. The as-synthesized $Cu_3Mo_2O_9$ sample by the surfactant-assisted hydrothermal method also exhibits a very obvious red-shifted PL emission. Generally, these results indicate that $Cu_3Mo_2O_9$ nanosheets prepared in this work are similar to high-crystalline hydrophilic surfaced $Cu_3(MoO_4)_2(OH)_2$ nanosheets, which have potential as a photoluminescent material.

[DOI: 10.22068/ijmse.3916]

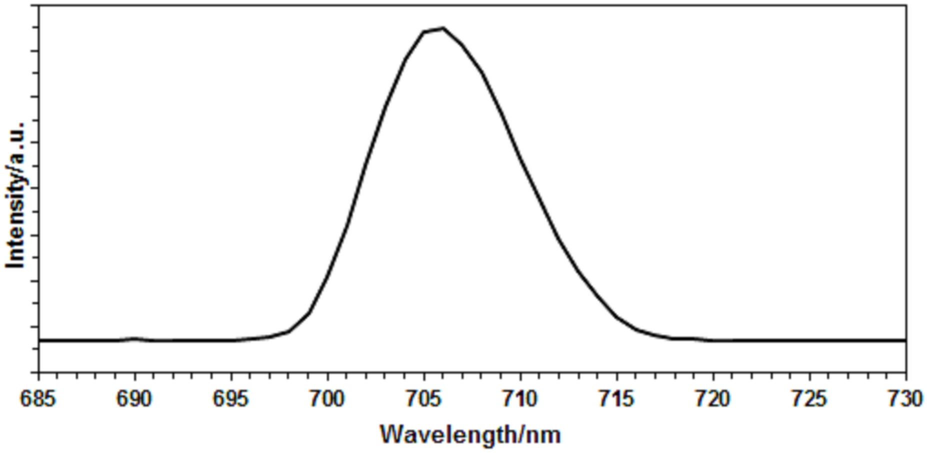

Fig. 10. Room-temperature photoluminescence spectrum of the $Cu_3Mo_2O_9$ nanosheets (calcined at 500 °C).

3.8 Magnetic Properties of $Cu_3Mo_2O_9$ Nanosheets

The magnetization of the as-prepared $Cu_3Mo_2O_9$ nanosheet sample at a calcination temperature of 500 °C as a function of magnetic field is shown in Fig. 11. The magnetization of this sample is not completely saturated yet at the maximum field of the measurements (15 kOe). Hysteresis loops at room temperature are much thinner and reveal that the as-synthesized sample exhibits zero coercivity and, thus, is superparamagnetic at room temperature. Moreover, the saturation magnetization M_s of as-synthesized $Cu_3Mo_2O_9$ is higher than that of as-synthesized $Cu_3(MoO_4)_2(OH)_2$ at room temperature.

[DOI: 10.22068/ijmse.3916]

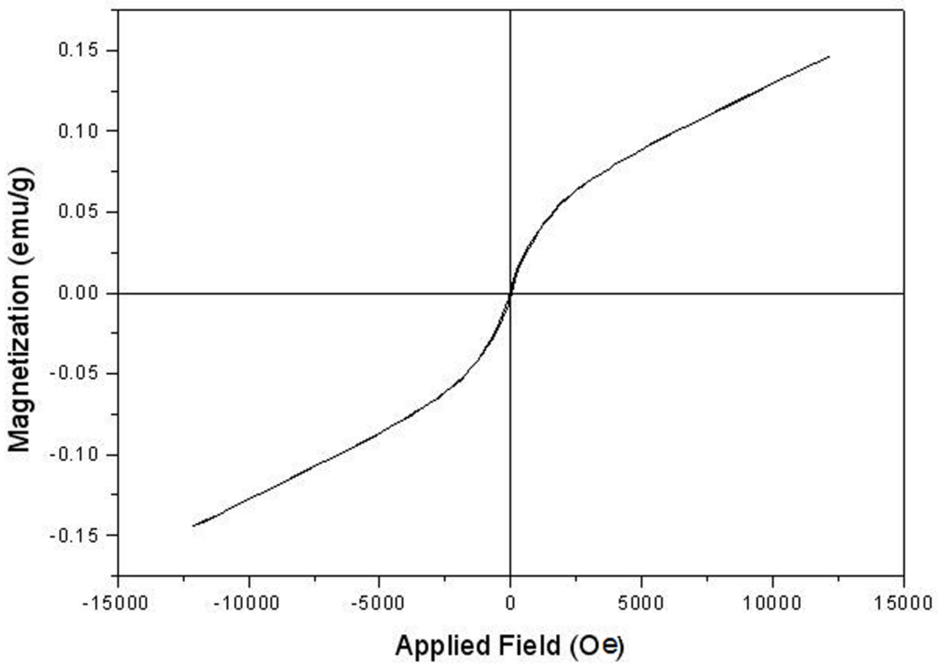

Fig. 11. Magnetic properties of the $Cu_3Mo_2O_9$ nanosheets: magnetization vs. field and hysteresis loops of sample at room temperature.

[DOI: 10.22068/ijmse.3916]

4. CONCLUSIONS

In this study, well-crystalline monoclinic $Cu_3(MoO_4)_2(OH)_2$ and orthorhombic $Cu_3Mo_2O_9$ nanostructures have been prepared *via* a simple and green route. This method is highly scale up able. The results demonstrated that well-crystallized Lindgrenite samples have rod morphology with diameters of about 100 nm, sheet form with a thickness of 30–100 nm and hollow sphere shape, consisting of a large number of nanosheets with a thickness of about 40-70 nm. The fabricated $Cu_3Mo_2O_9$ samples, obtained through the thermal treatment of Lindgrenite, retained their original morphologies. Furthermore, possible mechanisms for the formation of hydrophilic-surfaced $Cu_3(MoO_4)_2(OH)_2$ crystals are proposed. Possible proposed mechanisms of the $Cu_3(MoO_4)_2(OH)_2$ with various architectures were dominated by Ostwald ripening-oriented attachment, crystallization-dissolution-recrystallization and crystallization-dissolution-recrystallization-self-assembly growth mechanisms for nanorod, nanosheet and hollow sphere morphologies, respectively. Meanwhile, the photoluminescence and magnetic properties of the nanosheet samples have been investigated that the both of $Cu_3(MoO_4)_2(OH)_2$ and $Cu_3Mo_2O_9$ samples have super paramagnetic behavior at room temperature and in comparison with previous works, $Cu_3(MoO_4)_2(OH)_2$ and $Cu_3Mo_2O_9$ samples synthesized by the surfactant-assisted hydrothermal method in this work have a very obvious red-shifted PL emission and high intensity.

Acknowledgment. The authors acknowledge financial support of Tarbiat Modares University and Shahid Beheshti University for supporting this work.

[DOI: 10.22068/ijmse.3916]

REFERENCES

1. Zhang, L., Li, T., Deng, Y., Zhang, Y., Hu, S. and Sun,W., "$Cu_3Mo_2O_9$ nanosheet incorporated with hemoglobin on carbon ionic liquid electrode for the direct electrochemistry and electrocatalysis". J. Iran. Chem. Soc., 2014, 11, 407-414. https://doi.org/10.1007/s13738-013-0312-7.

2. Chu, W. G., Wang, H. F., Guo, Y. J., Zhang, L. N., Han, Z. H., Li, Q. Q. and Fan, S. S., "Catalyst-Free Growth of Quasi-Aligned Nanorods of Single Crystal $Cu_3Mo_2O_9$ and Their Catalytic Properties". Inorg. Chem., 2009, 48, 1243-1249. https://doi.org/10.1021/ic801885c

3. Palache, C., “Lindgrenite, a new mineral”. American Mineralogist: Journal of Earth and Planetary Materials, 1935, 20, 484-491.

4. lie, B. R., ping, K. Z., Min, G., Bin, Y., Hong, W. L. and Yang, H. H., “Hydrothermal Synthesis and Thermal Stability of Natural Mineral Lindgrenite”. Chem. Res. Chinese U. 2006, 22, 679-683. https://doi.org/10.1016/S1005-9040(06)60189-X

5. Alexandre, M., Beyer, G., Henrist, C., Cloots, R., Rulmont, A., Jérôme, R. and Dubois, P., “Preparation and Properties of Layered Silicate Nanocomposites Based on Ethylene Vinyl Acetate Copolymers”. Rapid Commun., 2001, 22, 643-646. https://doi.org/10.1002/1521-3927(20010501)22:8<643::AID-MARC643>3.0.CO;2-%23

6. Li, H., Chen, Y. and Xie, Y., “Photo-crosslinking polymerization to prepare polyanhydride/needle-like hydroxyapatite biodegradable nanocomposite for orthopedic application”. Mater. Lett., 2003, 57, 2848-2854. https://doi.org/10.1016/S0167-577X(02)01386-1

7. Xu, J. and Xue, D., “Hydrothermal synthesis of lindgrenite with a hollow and prickly sphere-like architecture”. J. Solid State Chem., 2007, 180, 119-126. https://doi.org/10.1016/j.jssc.2006.09.030

[DOI: 10.22068/ijmse.3916]

8. Vilminot, S., Andre, G., Plouet, M. R., Vigneron, F. B. and Kurmoo, M., “Magnetic Structure and Magnetic Properties of Synthetic Lindgrenite, $Cu_3(OH)_2(MoO_4)_2$”. Inorg. Chem., 2006, 45, 10938-10946. https://doi.org/10.1021/ic061182m

9. Xia, J., Song, L. X., Liu W., Teng, Y., Zhao, L. and Wang, Q. S. “Construction of $Cu_3Mo_2O_9$ nanoplates with excellent lithium storage properties based on a pH-dependent dimensional change” Dalton Trans., 2015, 44, 13450-13454.https://doi.org/10.1039/C5DT01645B

10. Butt, F. K., Cao, C., Ahmed, R., Khan, W. S., Cao, T., Bidin, N., Li, P., Wan, Q., Qu, X., Tahir, M. and Idrees, F., “Synthesis of novel ZnV_2O_4 spinel oxide nanosheets and their hydrogen storage properties”. CrystEngComm. 2014, 16, 894-899. https://doi.org/10.1039/C3CE41859F

11. [12]. Zhang, Y., Chenguo, H., B. Feng, X. Wang and Wan, B., “Synthesis and photocatalytic property of ZnSe flowerlike hierarchical structure”. Appl. Surf. Sci., 2011, 257, 10679-10685. https://doi.org/10.1016/j.apsusc.2011.07.078

12. Ohira, S., Sugawara, T., Nakajima K. and Shishido, T., “Synthesis and structural investigation of β-Ga_2O_3 nanosheets and nanobelts”. J. Alloys Compd., 2005, 402, 204-207. https://doi.org/10.1016/j.jallcom.2005.01.114

[DOI: 10.22068/ijmse.3916]

13. Sun, Y., Cheng, H., Gao, S., Sun, Z., Liu, Q., Lei, F., Yao, T., He, J., Wei, S. and Xie, Y., "Freestanding Tin Disulfide Single-Layers Realizing Efficient Visible-Light Water Splitting". Angew. Chem., Int. Ed., 2012, 51, 8727-8731. https://doi.org/10.1002/anie.201204675

14. Safdar, M., Wang, Z., Mirza, M., Butt, F. K., Wang, Y., Sun, L. and He, J. "Telluride-based nanorods and nanosheets: synthesis, evolution and properties". J. Mater. Chem. A, 2013, 1, 1427-1432. https://doi.org/10.1039/C2TA00470D

15. Hawthorne, F. C., Eby, R. K. and Neues J. b., Miner. Monats., 1985, 5, 243.
16. Calvert, L. D. and Barnes, W. H., "The structure of lindgrenite". The Canadian Mineralogist, 1957, 6, 31-51.

17. Jiang, W., Hua, X., Han, Q., Yang, X., Lu, L. and Wang, X., "Preparation of lamellar magnesium hydroxide nanoparticles via precipitation method". Powder Technol., 2009, 191, 227-230. https://doi.org/10.1016/j.powtec.2008.10.023

18. Tabrizi, S. A. H., Nassaj, E. T. and Sarpoolaky, H., "Synthesis of an alumina–YAG nanopowder via sol–gel method". J. Alloys Compd., 2008, 456, 282-285. https://doi.org/10.1016/j.jallcom.2007.02.044

[DOI: 10.22068/ijmse.3916]

19. Nguyen T. D. and Do, T. O., “Solvo-Hydrothermal Approach for the Shape-Selective Synthesis of Vanadium Oxide Nanocrystals and Their Characterization”. Langmuir, 2009, 25, 5322-5332. https://doi.org/10.1021/la804073a

20. Zhao, D., Yang, Q., Han, Z., Sun, F., Tang K. and Yu, F., “Rare earth hydroxycarbonate materials with hierarchical structures: Preparation and characterization, and catalytic activity of derived oxides”. Solid State Sci., 2008, 10, 1028-1036. https://doi.org/10.1016/j.solidstatesciences.2007.11.019

21. Yang, J., Sargent, E., Kelley, S. and Ying, J. Y., “A general phase-transfer protocol for metal ions and its application in nanocrystal synthesis”. Nat. Mater., 2009, 8, 683-689. https://doi.org/10.1038/nmat2490

22. Gibot P. and Laffont, L., “Hydrophilic and hydrophobic nano-sized Mn_3O_4 particles”. J. Solid State Chem., 2007, 180, 695-701. https://doi.org/10.1016/j.jssc.2006.11.024

23. Nguyen, T. D., Mrabet D. and Do, T. D., “Controlled Self-Assembly of Sm_2O_3 Nanoparticles into Nanorods: Simple and Large Scale Synthesis using Bulk Sm_2O_3 Powders”. Phys. Chem. C, 2008, 112, 15226-15235. https://doi.org/10.1021/jp804030m

24. Huang, P., Zhang, X., Wei, J., Pan, J., Sheng, Y. and Feng, B., “The preparation, characterization and optical properties of $Cd_2V_2O_7$ and $CdCO_3$ compounds”. Mater. Chem. Phys., 2014, 147, 996-1002. https://doi.org/10.1016/j.matchemphys.2014.06.050

25. Jiang, J.W., Fang, J., Fan, Z.Y., Yang, X. J., Lu, Q. T. and Hou, Y.B., "Synthesis of nano-sized tabular lindgrenite (Cu_3 (MoO_4) $_2(OH)_2$) by aqueous precipitation". J. Inorg. Mater., 2011, 26, 438-442. https://doi.org/10.3724/sp.j.1077.2011.10734

26. Luo, Z., Li, H., Shu, H., Wang, K., Xia, J. and Yan, Y., "Synthesis of $BaMoO_4$ Nestlike Nanostructures Under a New Growth Mechanism". Cryst. Growth Des., 2008, 8, 2275-2281.https://doi.org/10.1021/cg700967y

27. Nguyen, T. D., Dinh, C. T. and Do, T. O., "A general procedure to synthesize highly crystalline metal oxide and mixed oxidenanocrystals in aqueous medium and photocatalytic activity of metal/oxide nanohybrids". Nanoscale, 2011, 3, 1861-1873. https://doi.org/10.1039/C1NR10109A

28. Tang J. and Alivisatos, A.P., "Crystal Splitting in the Growth of Bi_2S_3". Nano Lett., 2006, 6, 2701-2706.https://doi.org/10.1021/nl0615930

29. Xu, J. and Xue, D., "Room Temperature Synthesis of Curved Ammonium Copper Molybdate Nanoflake and Its Hierarchical Architecture". J. Phys. Chem. B, 2006, 110, 17400-17405. https://doi.org/10.1021/jp0632788

[DOI: 10.22068/ijmse.3916]

30. Xu, J. and Xue, D., “Fabrication of Upended Taper-Shaped Cuprous Thiocyanate Arrays on a Copper Surface at Room Temperature”. J. Phys. Chem. B, 2006, 110, 11232-11236.https://doi.org/10.1021/jp061274x

31. Steiner, U. and Reichelt, W.,“A Reinvestigation of $Cu_3Mo_2O_9$, a Compound Containing Copper(II) in Compressed Octahedral Coordination”. Acta Cryst., 1997, C53, 1371-1373. https://doi.org/10.1107/S0108270197005751

32. Shi, R., Wang, Y., Zhou, F. and Zhu, Y., “$Zn_3V_2O_7(OH)_2(H_2O)_2$ and $Zn_3V_2O_8$ nanostructures: controlled fabrication and photocatalytic performance”. J. Mater. Chem., 2011, 21, 6313–6320. https://doi.org/10.1039/C0JM04451B

33. Nguyen, T. D., Mrabet, D., Dinh, C. T. and Do, T. O., “Biomolecule-assisted route for shape-controlled synthesis of single-crystalline $MnWO_4$ nanoparticles and spontaneous assembly of polypeptide-stabilized mesocrystal microspheres”. CrystEngComm, 2011, 13, 1450-1460. https://doi.org/10.1039/C0CE00091D

34. Mao, C. J., Geng, J., Wu, X. C. and Zhu, J. J., “Selective Synthesis and Luminescence Properties of Self-Assembled $SrMoO_4$ Superstructures via a Facile Sonochemical Route”. J. Phys. Chem. C, 2010, 114, 1982-1988.https://doi.org/10.1021/jp907525p

[DOI: 10.22068/ijmse.3916]

35. Gong, Q., Qian, X. F., Ma, X. D. and Zhu, Z. K., "Large-Scale Fabrication of Novel Hierarchical 3D $CaMoO_4$ and $SrMoO_4$ Mesocrystals via a Microemulsion-Mediated Route". Cryst. Growth Des. 2006, 6, 1821-1825.https://doi.org/10.1021/cg060133h

36. Chen, D., Tang, K. B., Li, F. Q. and Zheng, H. G., "A Simple Aqueous Mineralization Process to Synthesize Tetragonal Molybdate Microcrystallites". Cryst. Growth Des. 2006, 6, 247-252. https://doi.org/10.1021/cg0503189

37. Groenink, J. A., Hakfoort C. and Blasse, G., "The Luminescence of Calcium Molybdate". Phys. Status Solidi A, 1979, 54, 329-336. https://doi.org/10.1002/pssa.2210540141

38. Dinesh, R., Fujiwara, T., Watanabe, T., Byrappa K. and Yoshimura, M., "Solution synthesis of crystallized AMO_4 (A=Ba, Sr, Ca; M=W, Mo) film at room temperature". J. Mater. Sci., 2005, 41, 1541-1546. https://doi.org/10.1007/s10853-006-4634-z.

39. Ahmad, G., Dickerson, M. B., Church, B. C., Cai, Y., Jones, S. E., Naik, R. R., King, J. S., Summers, C. J., Kroger N. and Sandhage, K. H., "Rapid, Room-Temperature Formation of Crystalline Calcium Molybdate Phosphor Microparticles via Peptide-Induced Precipitation". AdV. Mater., 2006, 18, 1759-1763. https://doi.org/10.1002/adma.200600243

40. Sczancoski, J. C., Cavalcante, L. S., Joya, M. R., Varela, J. A., Pizani P. S. and Longo, E., "$SrMoO_4$ powders processed in microwave-hydrothermal: Synthesis, characterization

[DOI: 10.22068/ijmse.3916]

and optical properties". Chem. Eng. J., 2008, 140, 632-637. https://doi.org/10.1016/j.cej.2008.01.015

41. Wang, W. S., Zhen, L., Xu, C. Y. and Shao, W. Z., "Room Temperature Synthesis, Growth Mechanism, Photocatalytic and Photoluminescence Properties of Cadmium Molybdate Core−Shell Microspheres". Cryst. Growth Des., 2009, 9, 1558-1568. https://doi.org/10.1021/cg801194j

[DOI: 10.22068/ijmse.3916]